The International Journal of Advanced Manufacturing Technology (2023) 126:487–503
https://doi.org/10.1007/s00170-023-11072-2

ORIGINAL ARTICLE

Tribological assessment of the SiO_2 coating deposited by sol–gel process toward cutting tool coating

Natália Fernanda Santos Pereira[1,2] · Bárbara Cristina Mendanha Reis[3] · Anderson Júnior Dos Santos[4,5] · Manuel Houmard[6] · Marcelo Araújo Câmara[4] · Alessandro Roger Rodrigues[7] · Juan Carlos Campos Rubio[4]

Received: 28 October 2022 / Accepted: 3 February 2023 / Published online: 27 February 2023

Abstract

A more economic and thinner coating than the commercial ones was developed to improve the tribological behavior of high-speed steel (HSS) tools. This work focuses on performance of the SiO_2 coating was compared to uncoated HSS pins as well as coated ones (titanium nitride (TiN)) deposited by physical vapor deposition (PVD). The pin-on-disk test was carried out under a constant normal load of 10 N by applying sliding speeds of 40, 55, and 70 m·min^{-1}. The lowest values of the friction coefficient (μ) and the specific wear coefficient (k) were found for the coated pins. SiO_2 coating presented performance equivalent to the commercial TiN coating for the sliding speeds of 40 and mainly 55 m·min^{-1}, revealing a mild abrasive wear mechanism with the ferritic spheroidal graphite iron (SGI) interface surface. Thus, the sol-gel coating suggests being a promising protection for cutting tools submitted to abrasive wear when machining SGI workpiece at cutting speeds 3 times higher than those used with uncoated HSS tools, e.g., in drilling and tapping processes. Hereupon, SiO_2 is capable of substituting TiN coating for cutting speeds up to 55 m·min^{-1} with advantage of being an easier deposition process applied to any geometry without needing of high temperatures.

Keywords Tribology · Sol-gel process · Wear · SiO_2 · TiN · Cutting tool coating

✉ Natália Fernanda Santos Pereira
natalia.pereira@ifmg.edu.br

[1] Department of Production Engineering, Federal University of Minas Gerais, Av. Presidente Antônio Carlos, 6627, Belo Horizonte CEP: 31270-901, Brazil

[2] Department of Production Engineering, Federal Institute of Education, Science and Technology of Minas Gerais (IFMG - Campus Congonhas), Congonhas CEP 36415-000, Brazil

[3] Department of Urban Engineering, Federal University of Ouro Preto, Campus Morro do Cruzeiro s/n, Ouro Preto CEP: 35400-000, Brazil

[4] Department of Mechanical Engineering, Federal University of Minas Gerais, Av. Presidente Antônio Carlos, 6627, Belo Horizonte CEP: 31270-901, Brazil

[5] Department of Materials Engineering, Federal Center for Technology Education of Minas Gerais (CEFET – Campus 1), Belo Horizonte CEP 38150-510, Brazil

[6] Department of Chemical Engineering, Federal University of Minas Gerais, Av. Presidente Antônio Carlos, 6627, Belo Horizonte CEP: 31270-901, Brazil

[7] Department of Mechanical Engineering, University of São Paulo, Av. Trabalhador São-Carlense, 400, São Carlos CEP: 13566-590, Brazil

Nomenclature

P	Normal load
V	Sliding speed
S	Sliding distance
A	Wear track cross-sectional area
D	Wear track diameter
K	Specific wear coefficient
μ	Coefficient of friction
H	Hardness
E	Elasticity modulus
R_a	Arithmetic mean deviation
S_a	Arithmetic mean height
S_p	Maximum peak height
S_v	Maximum valley depth
S_{sk}	Skewness
S_{ku}	Kurtosis
S_p	Maximum peak height
S_v	Maximum valley depth

1 Introduction

Studies on thin films have experienced great increased given the diversity of applications for instance as light barriers, reflectors, storage means, corrosion resistant layers, adhesion improvement layers, conduction enhancement, and so on [1]. For this purpose, different coating techniques such as physical vapor deposition (PVD), chemical vapor deposition (CVD), electrochemical deposition, and sol-gel have been proposed [2]. Addressed efforts in this research field have led to the development of different organic/inorganic hybrid multifunctional coating materials such as sol-gel process for optic, electronic, ionic, mechanic, energy, environment, biology, and coating applications [2, 3].

In the last 20 years, the sol-gel technology has been successfully used because it allows the deposition of thin films (e.g., SiO_2, ZrO_2, Al_2O_3) with high hardness, good corrosion, and thermal resistances [4]. Especially, the sol-gel process is suitable to produce protective coatings in substrate of stainless steel, aluminum, copper, and magnesium [1, 5]. In addition, sol-gel thin films present excellent anti-wear and friction reduction performances under low loads [6].

Such technique produces 0.5 to 5 μm thickness oxides through hydrolysis and polycondensation reactions in water and co-solvent media [2, 7]. Among procedures of spraying, centrifugation, electrodeposition, and immersion, this latter is the most used due to its ability to cover complex geometries as well as simple deposition [4]. The advantages are easy performing, less dangerous, low cost, simple deposition equipment, easy deposition in large area, and easier to achieve the proper composition and applicability to broad substrates without any restriction [8, 9]. Some factors can affect the coating quality, such as hydrolysis ratio, acidity of the hydrolyzing agent, gelation and drying conditions, and types of solvent [2, 10]. Sol-gel method-based SiO_2 films have been used as thin coating for dielectric layer in microelectronic elements, anti-reflective, and protective coatings due to its chemical stability [11]. In addition, SiO_2 offers a low refractive index, protection against abrasion, enhanced mechanical resistance, and controllable porosity [12].

Amiri and Rahimi [2] applied sol-gel SiO_2 film on glass substrate and metal sheets for protecting against scratching and corrosion, respectively. Zhang et al. [13] analyzed the relationship between the preparation and its influence on the composition, structure, and tribological properties of two SiO_2 films deposited by sol-gel process derived from aqueous and ethanol solutions deposited on glass substrate. The aqueous solution-based SiO_2 film showed better performance given its wear resistance and lower friction coefficient while the ethanol solution-based SiO_2 film underwent severe brittle fracture, delamination, and significant wear debris resulting in high friction coefficient. On the contrary, only a few microfractures on the worn surface were observed for aqueous solution film.

Mora et al. [14] reinforced the sol-gel coating with nanoparticles of silica to improve mechanical properties and enhance the erosion and impact resistances. TiO_2/SiO_2 composite films prepared by sol-gel process can be used as protective layer on substrates of NiTi alloys as well as for bioactivity of implants in biomedical industry. The results indicated that films have higher electrochemical corrosion resistance [15]. Tlili et al. [4] found better tribological performance with less wear and damages in stainless steel coated with Al_2O_3 by sol-gel method for structural materials in various industrial sectors [4]. An Al_2O_3/SiO_2 nanocomposite coating was developed to protective against oxidation of hot-dip galvanized (HDG) steel by chemical immersion and sol-gel dip coating method. Al_2O_3/SiO_2 nanocomposite coating hindered oxidation of hot-dip galvanized steel [16].

Zhang et al. [17] investigate the modification of material FCI (flaky carbonyl iron) on the performance the corrosion and oxidation resistance when using particles coated by sol-gel method. The particles of material FCI was coating with a layer of Fe@SiO2@KH560@PDMS hybrid composite. The hybrid composite was elabored using lithium silicate (Li_2SiO_3), poly dimethyl siloxane (PDMS), and γ-(2,3-epoxypropoxy) propytrimethoxysilane (KH560). Particles coated with a hybrid layer provided excellent corrosion resistance and improved the thermal stability of the produced material in relation the oxidation.

Among several coating applications, successful mechanical machining processes in terms of productivity and quality depends strongly on tool coating and substrate. The cutting tools' market offers different options such as high-speed steel (HSS), carbides, ceramics, cubic bore nitride (CBN), and synthetic diamonds [18]. Because of the low cost and mainly high toughness compared to carbides [19], HSS substrates are widely used for drills, reamers, and taps since they work restricted inside holes and can be fractured by torsional stresses [18, 20]. Owing to the fact that the HSS has a lower critical temperature (~ 600 ºC), PVD coatings were originally developed for enhancing their performances [21]. In this way, hard films prepared by PVD process are frequently used since it reduces the friction, improves the hardness and wear resistance of the surfaces, and can work as a thermal barrier [22].

Rubio et al. [23] evaluated the performance of TiO_2 sol-gel coated HSS twist drills when cutting sandwich composite consisting of aluminum and polyethylene core (PEALL). The coated tool was better than uncoated one because it improved the hole quality, decreased its maximum diameter, and avoided the formation of build-up-edge of aluminum due to a lower friction coefficient. Rezende et al. [24] evaluated the performance of

TiO_2/Al_2O_3-coated multilayer tools prepared by sol-gel process. A better adhesion on the substrate was achieved because of the multilayer coating. The friction coefficient of the coated tool was lower for longer traveled sliding distances when compared with uncoated tools. Pereira et al. [25] drilled the ferritic spheroidal graphite iron (SGI) with coated HSS tools. Machining tests showed a performance 315% better for the SiO_2-coated tool when compared to the uncoated one. This coating also improved the hole quality by decreasing its surface roughness.

In conclusion, the main advantages of the sol-gel coating technique are its rapidity and capacity of coating any material and substrate geometry at low temperatures (< 400 °C) without requiring expansive and complex equipment. For these reasons, this process emerges as a promising method for low-temperature coating of the HSS substrates toward cutting tools. However, not much knowledge about the tribological behavior of sol-gel films was found in literature mainly for SiO_2 coatings on HSS substrate.

Therefore, the novelty this paper resides in compares and explains the tribological behavior of coated and uncoated AISI M2 HSS pins, one deposited by sol-gel process (SiO_2) and another by PVD method (commercial TiN). These pins were evaluated by sliding against SGI material, allowing analyses in terms of mechanical properties, friction coefficient, specific wear coefficient, and wear mechanisms.

2 Materials and methods

2.1 Characterization of the materials

A pin-on-disk tribometer Microtest model SMT-A/0100 was used to determine the friction and specific wear coefficients. The counter-face disk was a ferritic spheroidal graphite iron (SGI) grade 65–45-12 manufactured by casting process to comply with the ASTM A536-84 standard [26] having predominant matrix ferritic-pearlite and measurements of 52 mm × 50 mm testing area and 10 mm thickness. The chemical composition and mechanical properties of the disk are summarized in Table 1.

The disk arithmetic mean deviation (R_a) was measured with a Taylor Robson Surtronic 25 (0.36 ± 0.06 µm R_a) surface roughness tester which is lower than 0.8 µm as stated in the ASTM G99-05 standard [27] for pin-on-disk testing. A WPM 300/194 tester with 2.5 mm ball diameter and 62.5 kgf was used for Brinell hardness evaluation. Vicker's hardness tests were also performed by using a Wolper 62279 tester with 10 kgf loading, and 20 s indentation time in SGI specimen with revealed microstructure (4% Nital etching). A higher load was chosen so that micro-indenter covers as much of the matrix constituents' amount as possible in order to generate an average measurement and guarantee greater reliability in the result.

AISI M2 HSS material was used to manufacture spherical top pins as shown in Fig. 1a. HSS substrate pin (Fig. 1b) was characterized by Vickers microhardness tests was performed on a Shimadzu HMV-2 T tester with a load of 0.49 N and indentation time of 20 s. The value was of 835 ± 14 HV and is agreement with reported in the literature [28].

Prior to coating deposition, the pins were polished to reach 0.015 ± 0.004 µm R_a. The surfaces were ultrasonically cleaned (Branson model 1800) with ethanol for 30 min to avoid microscopic defects on the surface that affect the deposition quality. Figure 1c and d show the pins deposited by sol–gel (SiO_2) and PVD (commercial TiN) processes, respectively.

Table 1 Chemical composition (wt.%) and mechanical properties of the SGI disk

Chemical composition (wt.%)						
Fe	C	Si	Mn	P	S	Mg
93.68	3.63	2.47	0.09	0.06	0.01	0.06
Mechanical properties						
Tensile strength		Yield strength	Elongation		Brinell Hardness	Vickers hardness
554 MPa		376 MPa	14%		180 ± 6 HB	186 ± 7 HV

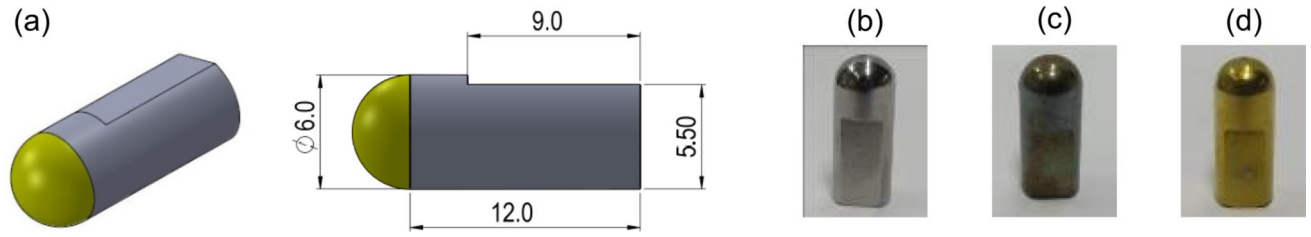

Fig. 1 **a** Dimensions of the spherical top pin (mm). **b** HSS substrate pin. **c** SiO_2-coated pin. **d** TiN-coated pin

SiO_2 coating was characterized by using the Scanning Electron Microscope (SEM) Quanta FEG 3D model equipped with Oxford Instruments X-Max Energy Dispersive Spectrometer (EDS). TiN coating was characterized by SEM Jeol JSMIT300 that includes the EDS analysis as well. The X-ray diffraction (XRD) was carried out for both coatings using a Philips-Panalytical diffractometer (model PW 1710) operated at 15–50 kV and monochromatized with Cu-Kα radiation (λ = 1.5406 Å) in which the scanning speed was 4 °·min^{-1} and interval of 20º–120º (2θ).

2D and 3D topographic images of the coatings were generated in the Atomic Force Microscope (AFM) Asylum Research-MFP-3D-AS model. Their analyses were performed with the Olympus AC240TS-R3 silicon probe (2 N·m^{-1} elastic constant, 70 kHz resonance frequency). The coatings roughness was characterized from the 2 µm × 2 µm areas by adopting the roughness parameters S_a (arithmetic mean height), S_p (maximum peak height), S_v (maximum valley depth), S_{sk} (skewness), and S_{ku} (kurtosis). S_p and S_v parameters were specified because they show peaks and valleys maximum amplitudes (not an average) with application in sliding coated surfaces under dynamic loading, i.e., cutting tools. Statistical roughness parameters skewness and kurtosis were chosen to evaluate the influence of the material concentration (or lack thereof) as well as the micro-asperities shape (spiky or bumpy) on the coated surface when in dynamic contact with SGI material.

Mechanical properties of the coatings were analyzed by means of nano-indentation on areas of 50 µm × 50 µm with spacing of 10 µm from each other in the pins' flat region (Fig. 1a). Hardness and elasticity modulus were obtained by using an Asylum Research MFP-3D-AS nano-indenter with Berkovich diamond tip according to the Oliver and Pharr [29]. Indentations located in 16 different positions on coatings were controlled to maximum loads of 0.5 mN for SiO_2 film (to avoid substrate interference) and 1.0 mN for TiN coating. The loading and unloading rates were 0.05 and 0.1 mN·s^{-1}, respectively for SiO_2 and TiN coatings with 10 s hold time at maximum load and 10 s for unloading. The indentation depth cannot exceed 10% of the film thickness though for some materials this percentage can reach 25% [30].

2.2 Sol–Gel coating

After cleaning, the pins were coated with three layers of sol-gel SiO_2 by the dip-coating deposition method. The reagents used to prepare the silica solution were the tetraethoxysilane (TEOS), deionized water, hydrochloric acid (HCl), and absolute alcohol as solvent. In solution, the concentration of silicon atoms corresponds to 2.35 mol·L^{-1}, the pH was 3.5, and the water/TEOS ratio was 2.2, in agreement with Houmard et al. [31]. The solution was aged for 48 h at room temperature and diluted to reach 1.5 mol·L^{-1}.

The dip-coating method applied in this research consisted of three steps: (i) immersion of the substrate into the sol–gel solution for 3 s; (ii) withdrawal at a constant speed of 0.5 mm·s^{-1} for drainage; (iii) drying at 80 °C for 15 min after each deposited layer which creates the silica thin film on the pin surface. These steps were repeated three times. After, the pins coated with silica were heated at 400 °C for 2 h to reduce the porosity and increase the density of the SiO_2 film. The coated pins were then gradually cooled inside the oven. Figure 2 shows a scheme of the dip-coating process.

2.3 Friction coefficient acquisition

The pin-on-disk tests were carried out according to the ASTM G99-05 [27] by using a tribometer Microtest model SMT-A/0100 as indicated in Fig. 3. Such test parameters were as follows: dry sliding wear condition, room

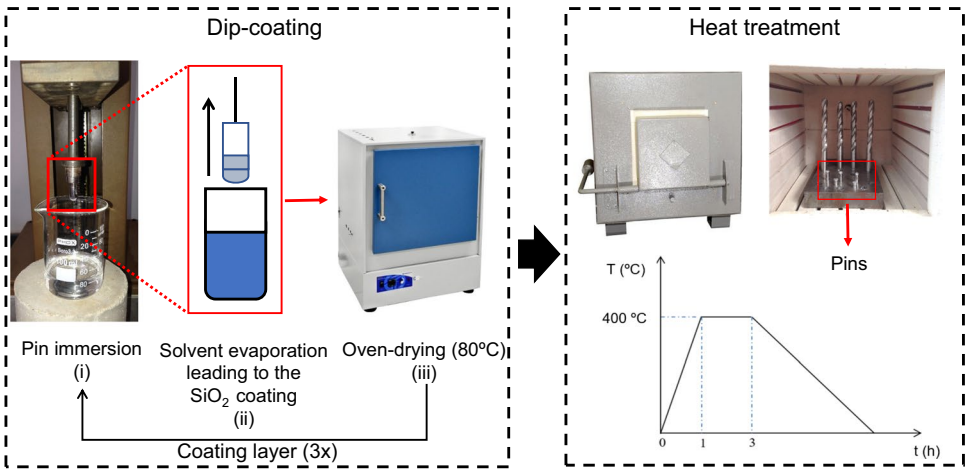

Fig. 2 Preparation steps of the SiO_2-coated pins by sol-gel technique

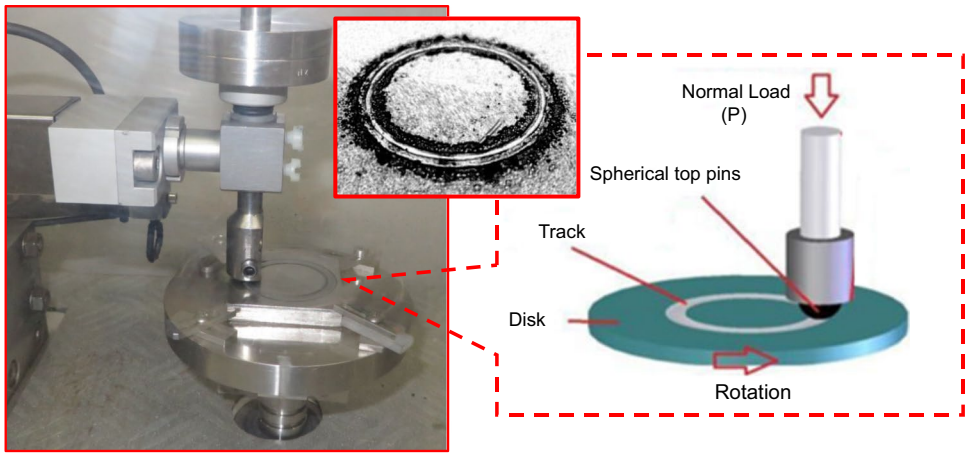

Fig. 3 Pin-on-disk friction and wear testing apparatus

temperature of 20 °C ± 1 °C, 10 N constant normal load, 480 rpm rotation, and 40, 55, and 70 m·min^{-1} sliding speeds. One replica was adopted for each condition and a new pin was used each time. Before each test, the working surfaces of the samples were ultrasonically cleaned (Branson model 1800) with ethanol for 30 min. After pin-on-disk tests, the same cleaning procedure was performed for the tribology analyses.

The track diameters were defined as 26.4 mm, 36.4 mm, and 46.4 mm corresponding to sliding speeds of 40, 55, and 70 m·min^{-1}, respectively. All tests were stopped at 600 m traveled distance which is in accordance with Holmberg [32]. Friction coefficient data were acquired through the Nanovea Tribometer software and average values were calculated after 400 m considering the signals steady state (constant level).

After each test, the wear tracks were analyzed to determine the specific wear coefficient (k) and thus evaluate the wear action of the pin contact on the SGI disk using Eq. (1). This equation was based on Archard and Hirst [33] which in turn is detailed by Feng et al. [34] and Souza et al. [35]. The specific wear coefficient (k) allows to compare the wear rates for different classes of materials [36].

$$k = \frac{\pi DA}{PS} \tag{1}$$

in which (k) is specific wear coefficient [mm^3/Nm], (D) is wear track diameter [mm], (A) is wear track cross-sectional area [mm^2], (P) is normal load [N], and (S) is traveled sliding distance [m]. The pins' wear rates were neglected due to their very low values of mass losses when compared to the SGI ones.

The stylus profilometer Hommel Tester T8000 and Hommelmap Expert 6.2 software were used to measure the wear track cross-sectional area (A) in three different regions on the same track. Such profilometer was also used to evaluate the wear on the surface of the pins and disk tracks after the tribometer tests. Worn tracks were characterized by SEM Jeol JSMIT300 equipped with EDS while worn pins were examined using SEM Quanta FEG 3D that includes EDS analyzer and so analyze the predominant wear mechanisms.

3 Results and discussion

3.1 Characterization of the coatings

Figure 4a shows the presence of Si and O elements confirmed by EDS, corresponding to the SiO_2 compound. SiO_2 film thickness ranges approximately from 490 to 550 nm (Fig. 4b), according to the SEM surface. EDS analysis of the substrate (Fig. 4c) indicates the expected chemical elements of the HSS composition, i.e., Fe, Si, Mo, Cr, and V.

As abovementioned, in this study, the sol–gel SiO_2 coating is compared to the commercial TiN deposited by PVD process (TiN Balinit A) provided by Oerlikon Balzers company. EDS analysis on coating indicates the presence of the Ti, N, and Fe atoms (Fig. 5a). The thickness film around 3.77 ± 0.08 µm is viewed in Fig. 5b. Mo, Cr, V, W, C, and Fe were identified on the substrate, corresponding to the HSS material, as shown in Fig. 5c.

X-ray diffractograms of the SiO_2 and TiN coatings are illustrated in Fig. 6. The investigation showed that the spectra presented peaks related to the substrate since the high intensity of the peaks of the crystalline structure of iron (α-Fe) was detected in the diffractograms. Besides, the presence of Fe_3W_3C carbide indicated by the Joint Committee on Powder Diffraction Standards (JCPDS card number 00–007-6760) was also identified by the diffractogram of the SiO_2 film (Fig. 6a). This happened because the X-ray beam passed through the thin sol-gel film reaching the substrate. Carbides formation in HSS substrate such as M_6C (Fe_3W_3C) is common and expected due to the stabilizing effect of C

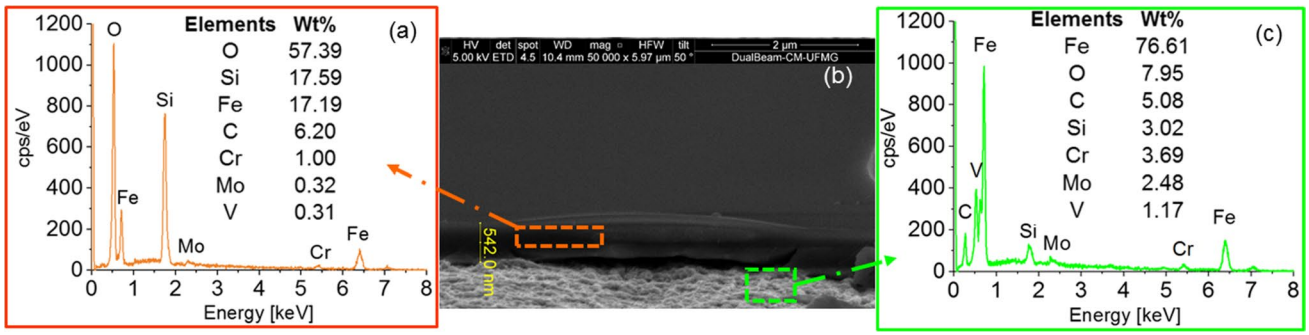

Fig. 4 **a** EDS spectrum from the pin coating. **b** SEM image of the pin cross-section showing the SiO_2 film. **c** EDS spectrum from the HSS substrate pin

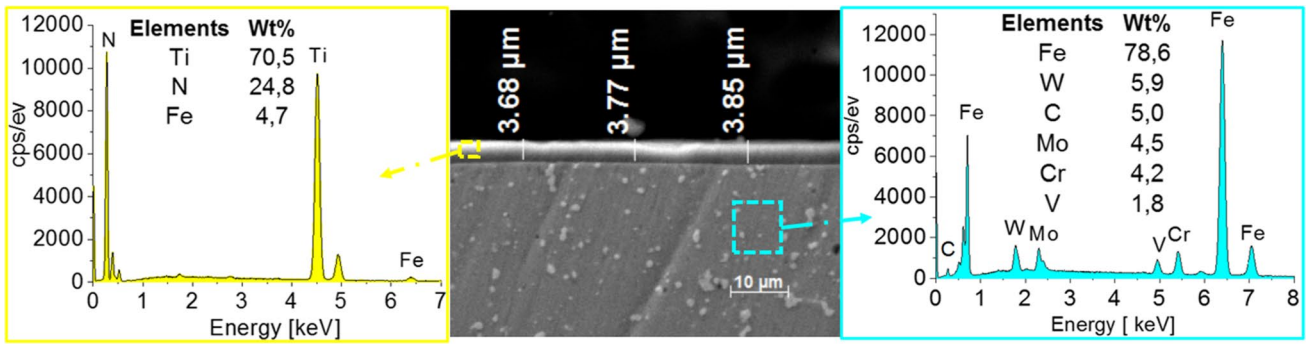

Fig. 5 **a** EDS spectrum from the pin coating. **b** SEM image of the pin cross-section showing the TiN film. **c** EDS spectrum from the HSS substrate pin

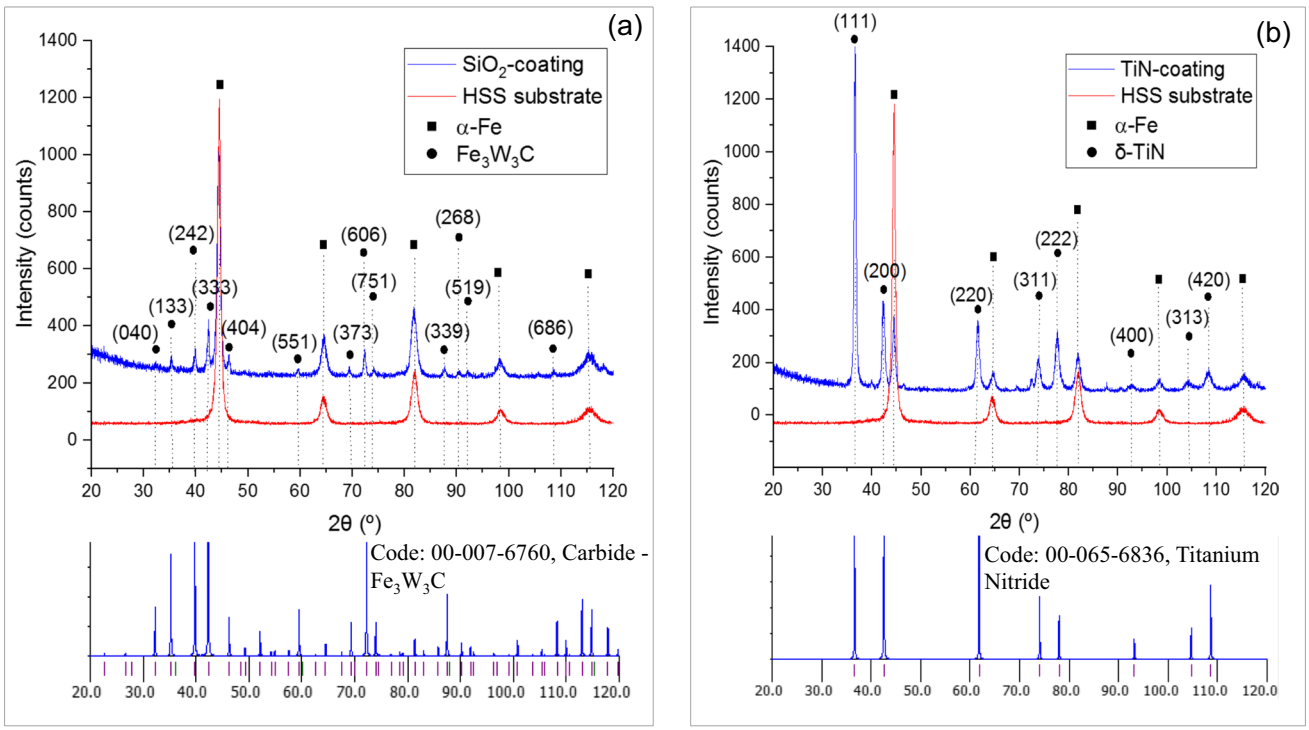

Fig. 6 X-ray diffraction spectra: **a** SiO_2. **b** TiN coatings. The spectra of the HSS substrate are presented in both figures for comparison (red lines)

combined with alloying transition metals, e.g., Cr, Mo, and W [37].

The X-ray diffractogram of the SiO_2-coated pin (Fig. 6a) indicates the absence of crystalline phases with silica atoms and confirms the amorphous state of the thin film. This is in agreement with X-ray diffraction patterns of sol-gel silica reported in the literature [38]. Figure 6b demonstrates that the diffraction peaks which are not related with the substrate phase match properly with the characteristic peaks of the TiN phase (JCPDS card number 00–065-6836), having a cubic crystalline structure in agreement with Tian et al. [39]. Thus, TiN coating presents the phase δ-TiN.

Figure 7 shows AFM 2D and 3D images of the SiO_2 and TiN films. The coating surfaces demonstrate to be completely covered forming uniformly distributed films free of damages. However, SiO_2 coating (Fig. 7a) exhibited higher topographic oscillations than the TiN-coated one (Fig. 7b) and this can be confirmed quantitatively by values of S_p and S_v roughness (Table 2). The relation of the roughness parameters with mechanism wear will be discussed in the Section 3.4.

Figure 8 presents nano-hardness testing by means of the load-unload vs. displacement curves. The SiO_2 coating (Fig. 8a) exhibited elastic behavior similar to that reported by Latella et al. [40], i.e., as indentation depth grows the curves move to the right, showing a relatively large variation. Thereby, the influence of the hard substrate over the coating is clearly evidenced [40]. For this reason, the hardness and elasticity modulus of the SiO_2 film were considered only for small indentation depths (100 nm or ~ 20% of the coating thickness) according to Xu and Rowcliffe [41]. Thus, the substrate presents an undermost influence on the nano-hardness measurements. Otherwise, TiN coating (Fig. 8b) display an elastoplastic behavior to low indentation depth, as observed by Bhowmick et al. [42]. As the indentation depth and the load increase, the substrate curves deviate from each other and form separate curve bands. However, the TiN coating curves closer with each other mean that deformation is mainly from the film, similar behavior reported by Bhowmick et al. [42].

The properties of hardness and elasticity modulus of the coatings are reported in Table 3. Such intervals of values were obtained from the load-unload vs. displacement curves showed in Fig. 8.

The mechanical properties coatings showed some variations in relation to that reported in the literature, mainly the

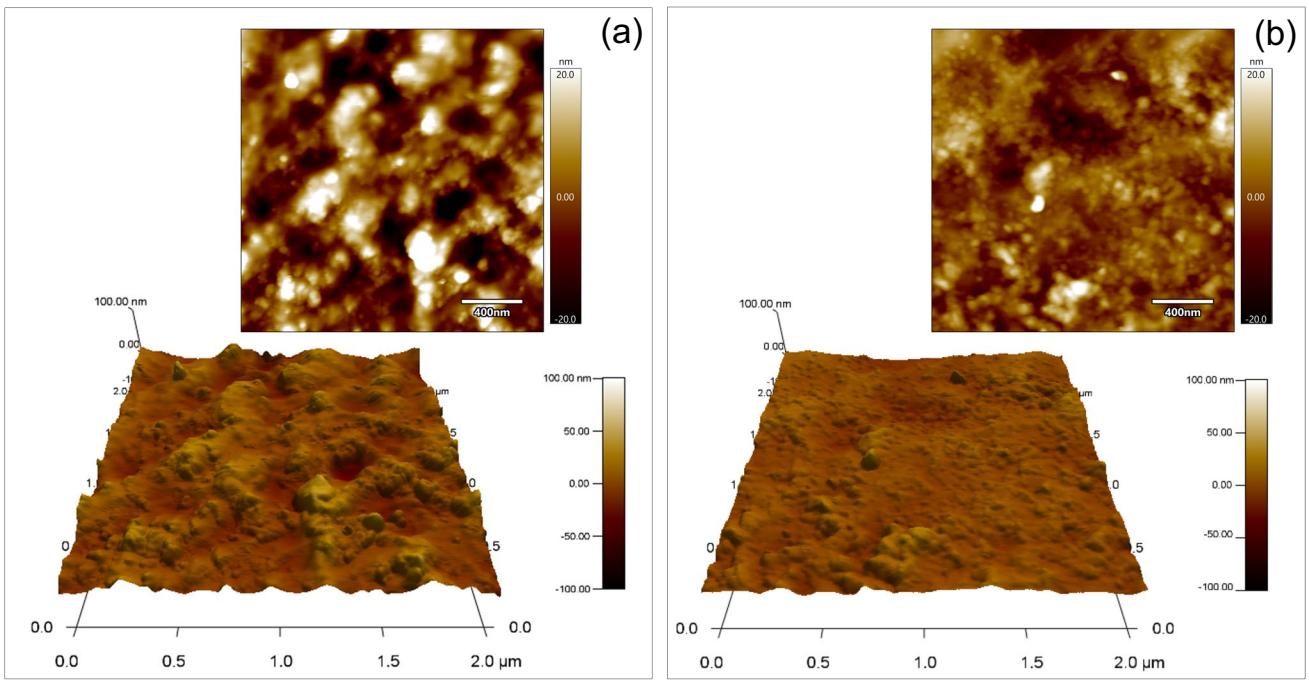

Fig. 7 AFM 2D and 3D images: **a** SiO_2. **b** TiN coatings

Table 2 Roughness parameters of the coatings

Coating	S_a	S_p	S_v	S_{sk}	S_{ku}
SiO_2	6.7 ± 1.4 nm	41 ± 3.0 nm	32 ± 5 nm	0.28 ± 0.01	1.36 ± 0.11
TiN	4.2 ± 1.1 nm	31 ± 2.0 nm	18 ± 4 nm	0.40 ± 0.02	0.91 ± 0.15

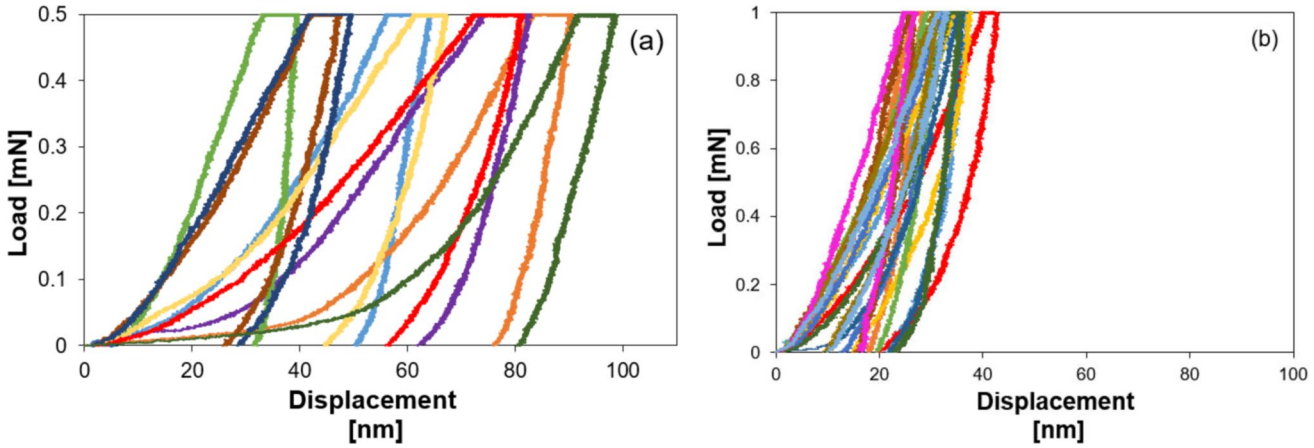

Fig. 8 Load-unload vs. displacement curves: **a** SiO_2. **b** TiN

Table 3 Mechanical properties of the substrate and coatings from this paper and literature

Surface	H [GPa]	E [GPa]	H^3/E^2 [GPa]	Ref.
SiO_2	2.7–4.7	54–128	0.007–0.006	This paper
	1.8–3.0	80–200	0.001–0.0007	[43]
TiN	36.3–44.3	585–625	0.139–0.222	This paper
	35.0–45.0	450–550	0.212–0.301	[39, 42]

H hardness, *E* elasticity modulus

elasticity modulus. However, hardness as well as many other properties of coatings are greatly affected by their design that includes chemical and phase composition, microstructure, amount and density of layers, relative thickness, grain size, and chemical bonding between atoms [42, 44, 45, 46]. Lastly, it can also be observed that the SiO_2 film is more ductile and more elastic than TiN coating since H^3/E^2 ratio for TiN coating is higher than for silica one which means that TiN film presents higher resistance to plastic deformation and wear [47].

3.2 Tribology performance

The evolution of the friction coefficient (μ) as a function of sliding distance from the pin-on-disk tests are shown in Fig. 9a, b, and c up to 600 m traveled distance. Average values with error bars of the friction coefficients after a sliding distance of 400 m are synthetized in Fig. 9d.

The friction coefficient curves show different behavior after the running-in periods. It is interesting to note that all testing for the HSS substrate showed a substantial increase in the friction values in the initial sliding distances up the stable region (after 300 and 400 m), with greater instability and fluctuations. This behavior is probably due to the presence of debris (wear particles) at the interface due to the detachment and temporary sliding of the transferred material built-up between the mating surfaces, as observed in the Grzesik et al. [48]. This debris then creates a third element, which induces a rapid transition in friction [49].

Differently for SiO_2 and TiN coatings, friction coefficient curves were more stable over the traveled distance. In the initial sliding distances, the friction coefficient value increases and stabilizes in the stable region of the curve. However, to SiO_2 coating at a sliding speed of 70 $m{\cdot}min^{-1}$, the friction coefficient curve showed higher instability, smaller running-in periods, and a rapid increase in friction coefficient values.

It is well known that low friction corresponds to low wear and consequently high friction to higher wear [50]. Additionally, higher friction coefficient and specific wear coefficient were found for the pair corresponding to the HSS substrate pin in all sliding speeds showing that wear was clearly more severe for this tribological pair (Table 4). According to Hutchings and Shipway [36], the specific wear coefficient for metals and ceramics is typically below 10^{-4} to 10^{-5} mm^3/Nm at mild wear conditions and varies from 10^{-3} to 10^{-2} mm^3/Nm for severe wear. The values presented in Table 4 are consistent with Hutchings and Shipway [36] and Grzesik and Rech [50], i.e., the lowest friction coefficients for SiO_2 and TiN coatings correspond to lower wear rates (bold values).

SiO_2 and TiN coatings confirmed their superiority in terms of wear resistance since they caused lesser wear to SGI when compared to pair contend the HSS substrate. SiO_2 coating reduced friction coefficient up to 55% while TiN up to 63% when compared to the HSS substrate pin for the sliding speeds stablished in trials. However, differences were determined in the friction coefficients as the sliding speed varied. For the SiO_2-coated pin when the sliding speed increases from 40 to 55 $m{\cdot}min^{-1}$, the friction coefficient

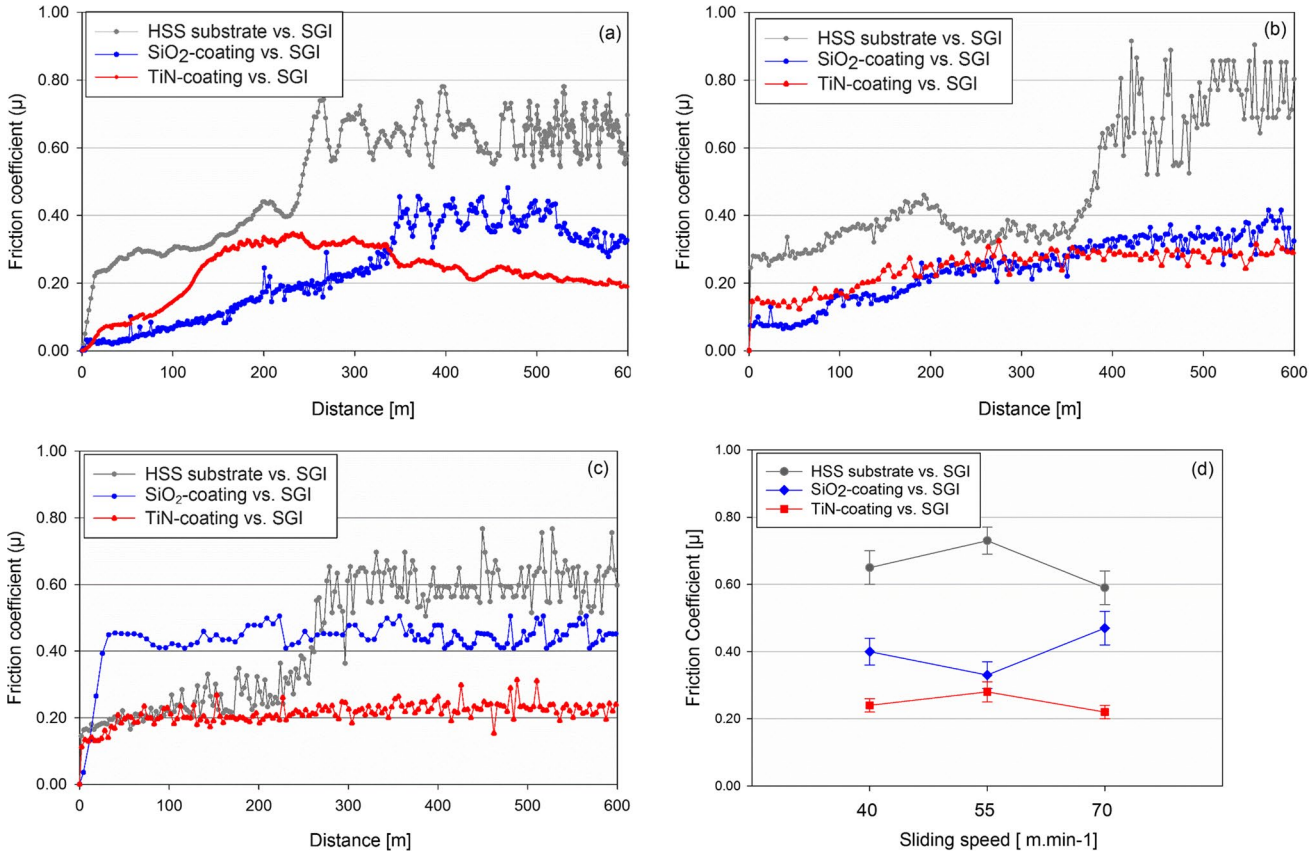

Fig. 9 Friction coefficient curves of the HSS substrate, SiO_2-coating, and TiN-coating pins on the SGI counter-face disk at sliding speeds of **a** 40 m min^{-1}, **b** 55 m min^{-1}, and **c** 70 m min^{-1}. **d** Grouped average values of the friction coefficients

Table 4 Friction coefficient (μ) and specific wear coefficient (k) of the tribological pairs tested

Pin	μ			k [10^{-5} mm^3/N m]		
	Sliding speed [m·min^{-1}]			Sliding speed [m·min^{-1}]		
	40	55	70	40	55	70
HSS substrate	0.65 ± 0.05	0.73 ± 0.04	0.59 ± 0.05	226 ± 0.10	410 ± 0.20	757 ± 0.10
SiO_2	0.40 ± 0.04	**0.33 ± 0.04**	0.47 ± 0.05	1.13 ± 0.10	**1.10 ± 0.04**	329 ± 0.10
TiN	0.24 ± 0.02	0.28 ± 0.03	**0.22 ± 0.02**	3.41 ± 0.20	0.26 ± 0.06	**0.21 ± 0.02**

The bolded values indicate lower wear rates

decreases. Similar behavior took place for HSS substrate and TiN-coated pins when the sliding speeds varied from 55 to 70 m·min^{-1}. In literature, ceramic-based films behave like a self-lubricant between pin and substrate, and thus contribute to decrease the friction [5]. Rabinowicz et al. [51] reported that friction coefficient reduces due to the low interface shear stress and the high temperature, which encourage oxide formation and produce a mild wear. This low shear stress allows to oxidize wear particles and thus they are removed from the surface as oxides. However, an increase in the friction coefficient and the specific wear coefficient was observed when analyzing the SiO_2 coating for 70 m·min^{-1}. This indicates that the SiO_2 coating has a worse anti-wear condition to higher sliding speed than 55 m·min^{-1}.

It is interesting to note that SiO_2 coating presented equal and superior performance, respectively, in terms of friction coefficient (μ) at 55 m·min^{-1} and specific wear coefficient (k) at 40 m·min^{-1} sliding speeds when compared with TiN film (Table 4). These speeds are 3 times higher than those usually applied to drill or tap casting irons by using uncoated HSS, as well as equivalent to that for TiN-coated HSS [50, 52]. Thus, in these cases, more expensive commercial coatings can be substituted by SiO_2 sol-gel technique which is cheaper and easier to process. In contrast, this finding

suggests that SiO_2 as cutting tool coating should not be employed for higher cutting speeds than 55 m·min^{-1} because its performance in terms of friction and wear rate worsens.

3.3 Analysis of the worn tracks

Figure 10 shows typical cross-sectional profiles of the wear tracks obtained from the counter-face SGI after the pin-on-disk test against uncoated and coated pins. HSS substrate pin induced a higher wear (deep tracks) on surface of the SGI in all sliding speeds tested. SiO_2 coated pin produced a similar wear behavior at sliding speed of 70 m·min^{-1} (Fig. 10c). It clearly shows a severe wear on these tracks, so that it can be related to the increase of the specific wear coefficient (k) (Table 4).

In addition, the narrowest and shallower wear tracks were obtained for the TiN-coated pin for all sliding speeds whilst the SiO_2 film behaved very close to TiN coating at 40 and 55 m·min^{-1}. This indicates a wear resistance of the SiO_2 film for lower sliding speeds. Similar results were found by López et al. [53] when wear experiments were carried out on sol-gel silica coatings. In sliding wear, whereas a fraction wear particles generating a lot of third bodies (or tribomaterial) are preferentially ejected from the contact region as discussed by Fillot, Iordanoff, and Berthier [54] another part, wear particles maybe adhere to the surface and get trapped in wear troughs or incorporated into films adhering to the surfaces of the first bodies [55]. And therefore, may even act as solid or solid/liquid lubricant and allow for smaller rates of materials lost as observed to the TiN-coated pin for all sliding speeds and SiO_2 coated pin for lower sliding speeds (40 and 55 m·min^{-1}).

Upper view SEM images of the wear tracks produced on the SGI disk with different sliding speeds are also shown in Fig. 11.

SEM images from Fig. 11 confirm that coated pins induced smoother wear, which suggests a mild abrasive wear. Narrower scratches in the worn track could were formed by the wear debris that was released as a result of a break in passive oxide layer and contribute to contact abrasion.

However, the contact of HSS substrate pin for all sliding speeds and SiO_2-coated pin for 70 m·min^{-1} showed evidence of plowing, plastic deformation and smooth scratches in sliding direction in the worn tracks of the SGI disk.

Therefore, the wear was clearly more severe on these tracks. In the sliding surfaces, interactions can mainly lead to four main groups of wear mechanisms accepted: adhesion, abrasion, surface fatigue, and tribochemical reactions that can occur in a more or less pronounced form [56]. However, it likely that to plastic deformation increase the area of contact [36] and favor generate a transfer layer characteristic of adhesion mechanisms. This result is consistent with presence of greater amount of transferred material on the SiO_2-coated and HSS substrate pins for the testing conditions aforementioned (see Section 3.4).

Table 5 summarizes the elemental composition registered from the EDS spectra of the worn tracks produced on the SGI counter-face disk after the pin-on-disk testing. The results indicate the presence of Fe, O, C, and Si that are typical elements of the SGI but none transfer of material from pins to tracks was found. Furthermore, an increase in the oxygen content was detected on worn tracks of the HSS substrate (39.1%, 40.5%, and 43.0%) and SiO_2 coating (43.5%) such as highlighted in Table 5 (bold values). This demonstrates that the SGI tracks' surfaces were slightly oxidized, which was also observed by Souza et al. [35]. This may be associated higher friction contact temperature is reached on the worn surfaces at high speed sliding and encourage oxide formation as reported by Rabinowicz et al. [51]. However, a disadvantage the oxide layer can turn into debris due to its high hardness and brittleness and contribute to contact abrasion [34]. This fact is consistent with presence of smooth scratches in the worn track of HSS substrate and SiO_2 coating for 70 m·min^{-1}.

Then, the oxide surface layer is removed by repeated and multiple contacts by generating wear debris which are trapped between the tribo-pairs' contact surfaces. This continuous removal process of layers and their reformation may result in the thickening of the oxide layer [57].

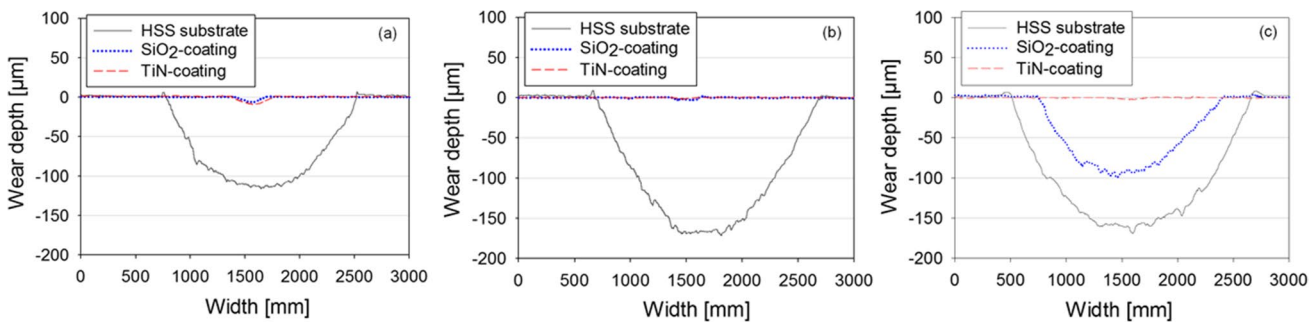

Fig. 10 Wear tracks profile at the end of the pin-on-disk tests under sliding speeds of **a** 40 m·min^{-1}, **b** 55 m·min^{-1}, and **c** 70 m·min^{-1}

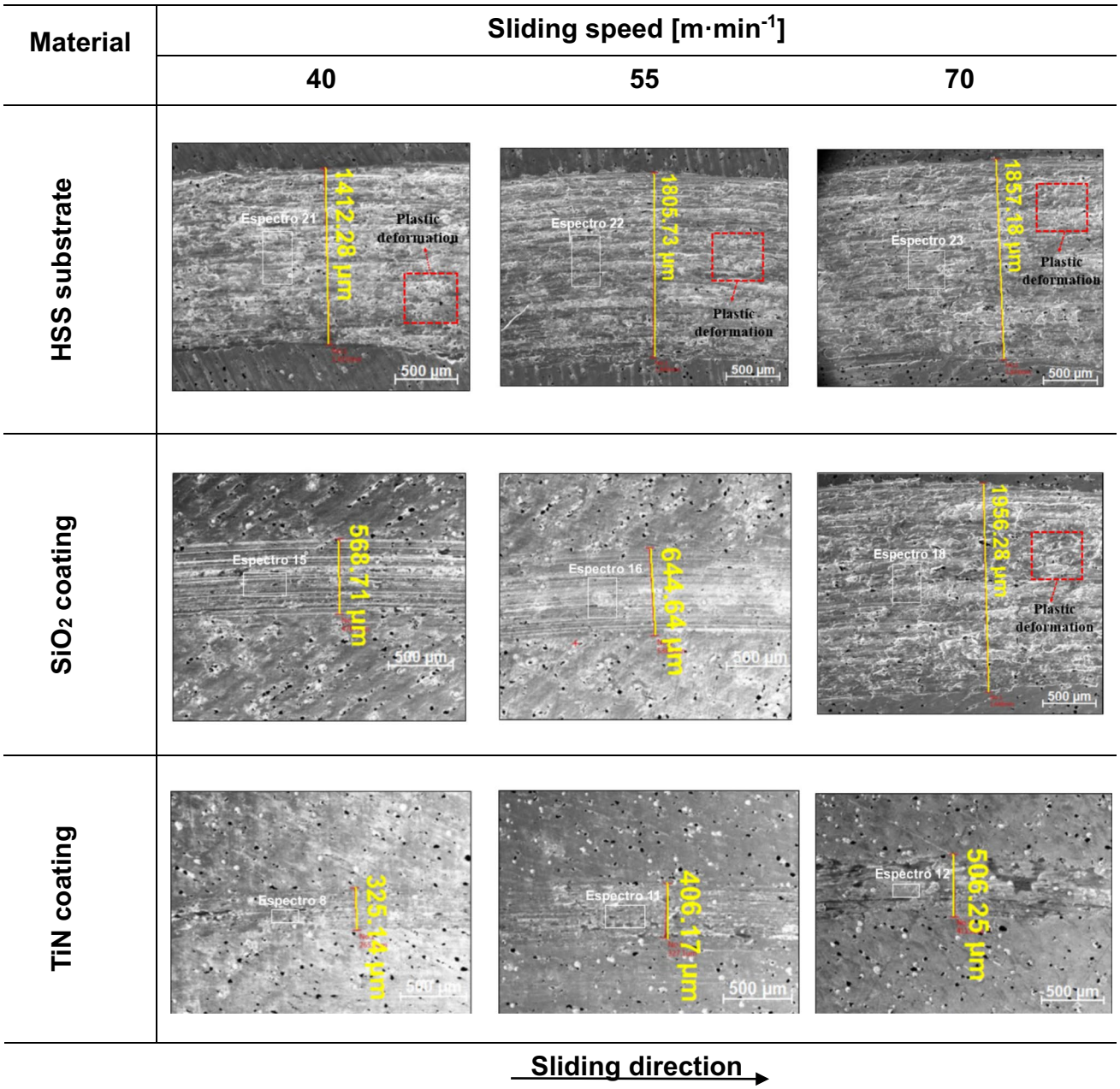

Fig. 11 SEM images of the worn tracks' upper views generated on the SGI disk at sliding speeds of 40, 55, and 70 m·min^{-1} and for HSS substrate, SiO_2 coating, and TiN coating

This compacted layer formation and adhesion nature can facilitate its transfer to the pin surface which in turn can hardens (work-hardening) [58] and increase the specific wear coefficient.

3.4 Analysis of worn pins

Three-dimensional maps, SEM images, EDS spectra, and chemical compositional maps of the worn pins at the end of the pin-on-disk tests are shown in Figs. 12, 13, and 14. EDS spectra show the presence of Fe, Si, C, and O in the worn regions and the chemical maps indicated higher presence of C and formation of the transfer layer was observed, which suggest be of the disk material to HSS substrate pin for all sliding speeds tested (Fig. 12a, b, and c). Despite the elevated hardness of the pin substrate (835 ± 14 HV), the behavior of this tribological pair was governed by the adhesion wear mechanism with the intense plastic deformation (worn

Table 5 EDS analysis of the worn tracks produced on the SGI counter-face disk

Pins	Sliding speed [m·min^{-1}]	EDS spectrum	wt.%			
			Fe	O	C	Si
HSS substrate	40	21	51.2	**39.1**	8.8	1.0
	55	22	49.0	**40.5**	9.5	1.0
	70	23	45.3	**43.0**	10.9	0.9
SiO_2	40	15	58.9	34.0	5.9	1.3
	55	16	59.8	33.3	5.5	1.3
	70	18	44.4	**43.5**	11.2	0.9
TiN	40	8	64.8	30.1	3.8	1.3
	55	11	64.9	30.0	3.6	1.5
	70	12	63.2	31.2	4.3	1.4

The bolded values highlight highest oxygen content

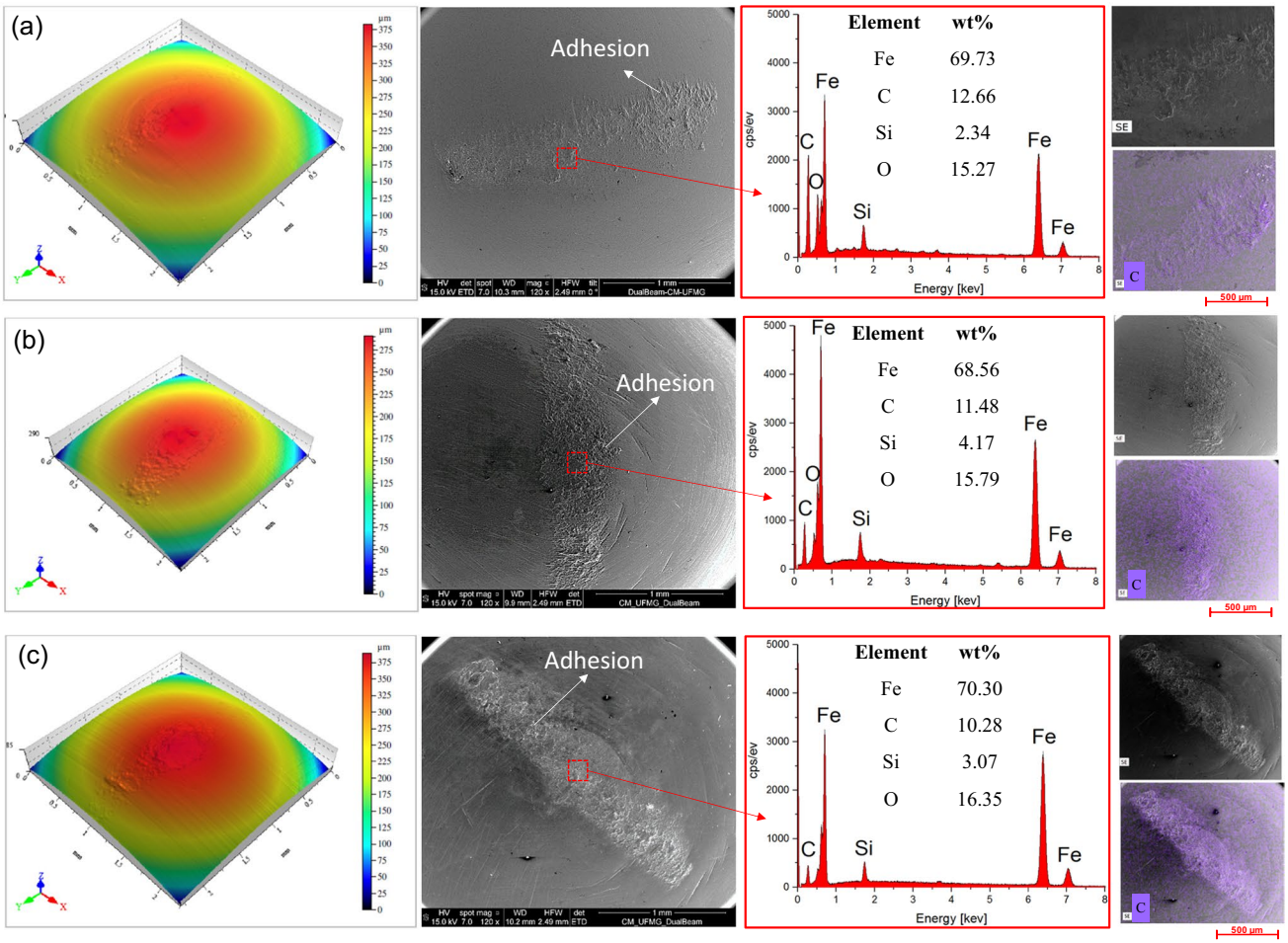

Fig. 12 Three-dimensional maps, SEM images, EDS spectra, and chemical compositional maps of the HSS substrate pins' wear regions against SGI at **a** 40 m·min^{-1}, **b** 55 m·min^{-1}, and **c** 70 m·min^{-1} sliding speeds

track) influenced by SGI hardness (180 ± 6 HB/186 ± 7 HV), in this case, sliding against a soft material.

Adhesion mechanism means that strong interatomic bonds between contacting solids whenever atoms come into intimate contact [51]. If the resist the shear force the interatomic bonds is higher than the strength of the base material, force the fracture in the weaker material, resulting in material transfer from one body to the other [36]. Besides, this type of mechanism explains the behavior of the friction coefficient curves, which increased after from a

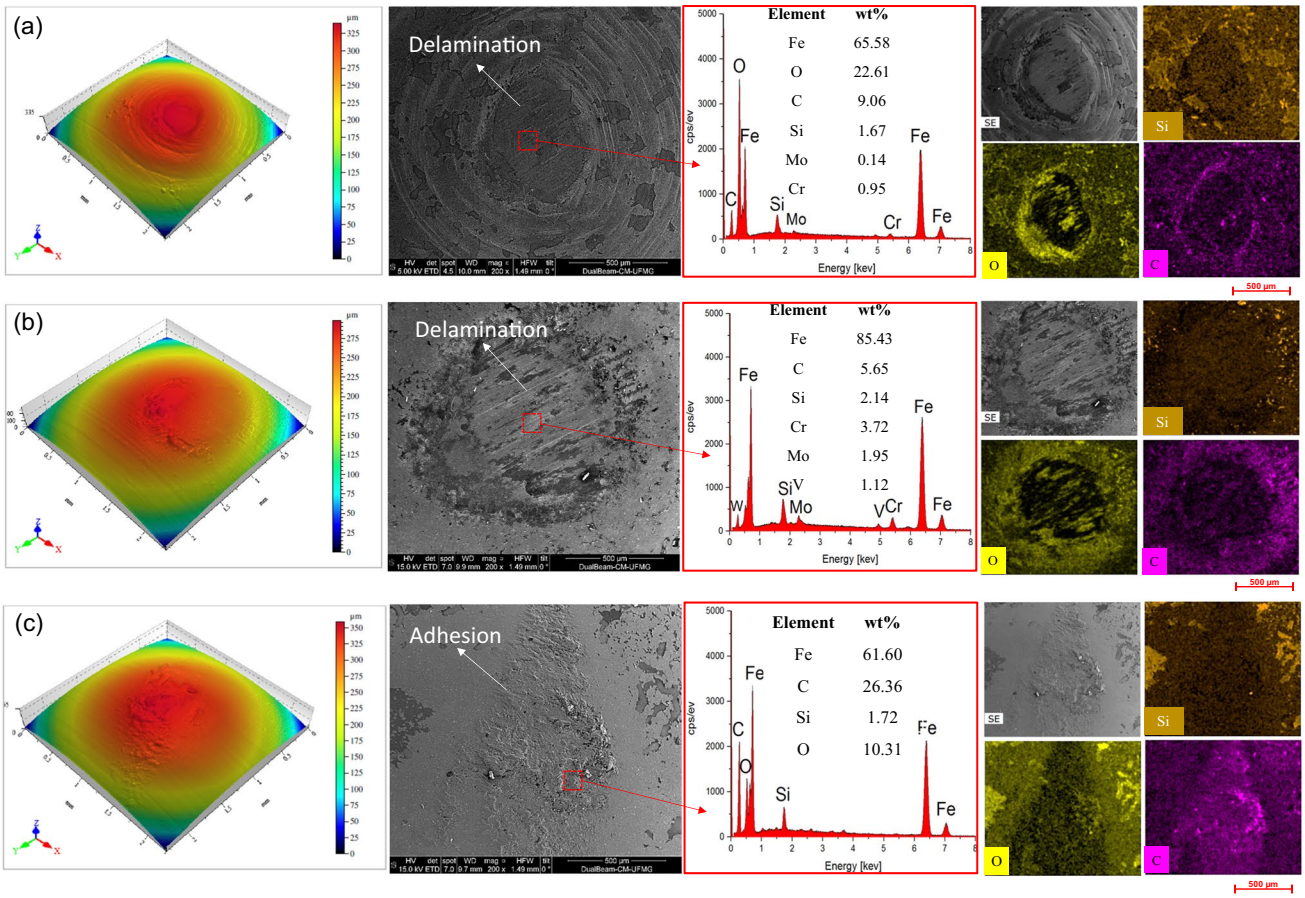

Fig. 13 Three-dimensional maps, SEM images, EDS spectra, and chemical compositional maps of the SiO_2-coated pins' wear region against SGI at **a** 40 m·min^{-1}, **b** 55 m·min^{-1}, and **c** 70 m·min^{-1} sliding speeds

sliding distance of 300 and 400 m. These findings support the hypothesis of large interaction between HSS substrate pin and SGI counter-face disk which resulted in higher friction and specific wear coefficients (Table 4).

As for wear of the SiO_2-coated pin, three-dimensional maps and SEM images (Fig. 13a and b) show the coating delamination given the substrate exposure. EDS spectra from the wear zone indicate the chemical elements Fe, W, Mo, Cr, and V which belong to the HSS composition (substrate). The chemical compositional mapping reveals a slight reduction in the amount of Si on the worn region which evidences a higher delamination of the coating. Thus, suggest this delamination were generated by abrasive wear mechanism enhanced by debris' movements which produced narrow scratches on the SGI wear track (Fig. 11). On the other hand, although the coating has delaminated, the lowest friction and specific wear coefficients were measured for moderate sliding speed (Table 4), demonstrating that the coating protected the substrate from the action of the SGI counter-face disk for 600 m traveled distance in the pin-on-disk testing.

The wear mechanism for 40 and 55 m·min^{-1} (delamination followed by abrasion) can have been influenced by nanometric thickness of the silica coating in relation to the peak-valley roughness ($S_v + S_p$). According to Table 2, maximum roughness can reach 81 nm which represents about 16% of the film thickness. This proportion can have favored the film delamination since coating thickness is sub-micrometric (490–550 nm). This hypothesis could be verified by increasing the coating thickness or decreasing the film roughness. No thermo-chemical effect should be considered given that sliding speeds were lower and no transfer layer was observed in the analyzed pin's region which in turn would lead to adhesion wear mechanism.

Differently from 40 and 55 m·min^{-1}, the wear mechanism at highest sliding speed was diverse and more severe such as shown in Fig. 13c. According to the three-dimensional mapping and SEM images, the transfer layer was observed. The presence of Fe, C, Si, and O detected by EDS spectra and chemical compositional maps suggests transference of the disk material on coated pin.

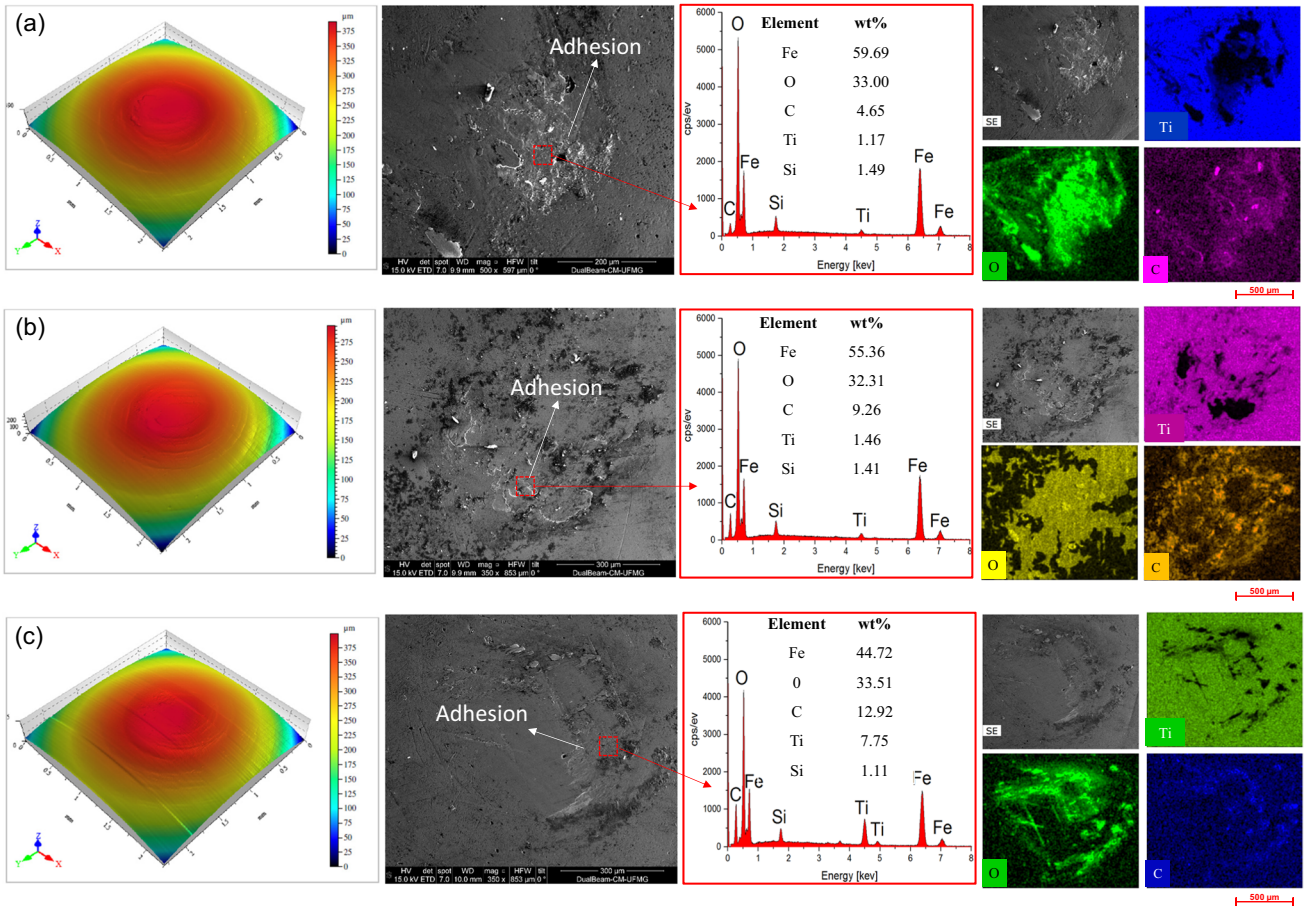

Fig. 14 Three-dimensional maps, SEM images, EDS spectra, and chemical compositional maps of the TiN-coated pins' wear region against SGI at **a** 40 m·min^{-1}, **b** 55 m·min^{-1}, and **c** 70 m·min^{-1} sliding speeds

The symmetry and distribution of the coating micro-irregularities (roughness) can have collaborated with the adhesion wear mechanism once $S_{sk} = 0.28$ and $S_{ku} = 1.36$, i.e., SiO_2 surface presents prevalence of peaks ($S_{sk} > 0$) with bumpy peaks and valleys ($S_{ku} < 3$) [59, 60]. Surfaces empty of material (more peaks) reduce the contact area with its tribological pair and increase the contact pressure [60] contributing to the adhesive bonds and adhesion wear mechanism [61] which are more significant for lower elasticity modulus (around 100 GPa) such as of the silica coating (Table 3).

However, the highest sliding speed led to plastic deformation and increase in the tangential force (due to friction). The tangential force must generate enough tension to break the joint points formed during contact pin-on-disk [35]. Thus, the adhesion break between the surfaces can cause loose particles remain dispersed in the sliding interface acting as abrasives bodies and can lead to the delamination of the silica coating, since the SiO_2 films are thin. The worn track with smooth scratches (Fig. 11) suggests the participation that abrasive particles that may be due to the delamination or chipping. Moreover, the behavior of the friction coefficient curves showed higher instability, a smaller running-in period and followed by a quick rise in the friction coefficient values that could be associated with coating wear-through. However, for this condition, suggest that the adhesion mechanism, plastic deformation, and delamination of the film led to a severe wear regime enhanced by low hardness of the SGI material and lower elasticity modulus of the SiO_2 coating.

Lastly, Fig. 14 shows through the three-dimensional maps and SEM images that TiN-coated pin presented lower level of wear at the end of pin-on-disk testing. EDS spectra and chemical compositional mapping indicate the presence of Ti (especially chemical maps) demonstrating that the coating was not delaminated. The presence of O, C, Fe, and Si suggest the transference from the disk surface material to the pin. The area covered by transferred material is clearly smaller, and thus, a minimal adherence for this tribological pair was detected which was also influenced by greatest elasticity modulus and hardness of the TiN (lesser strain under loading). The higher elasticity modulus led lower the elastic deformation and causes a reduction in the real area of contact between the disk and the pin [62]. This result validates that the TiN coating presents less surface interaction

with SGI which corroborate the values of the friction and specific wear coefficients (Table 4) as well as higher H^3/E^2 ratio (Table 3), confirming higher wear resistance and higher resistance against plastic deformation found to this tribological pair.

When analyzing roughness parameters for TiN coating, it is noticed that the proportion between peak-valley amplitude ($S_p + S_v = 55$ nm) and film thickness (3.77 µm) is 10 times lesser than for SiO_2 coating (1.5% against 16%). Besides, S_p and S_v roughness values for TiN are, respectively, 25% and 44% lesser than for silica coating. These topographic characteristics aided by mechanical and tribological properties (harder and lesser friction) led to the wear mechanism for slight adhesion instead of coating delamination. The influence of the skewness and kurtosis was the same for SiO_2 coating, i.e., $S_{sk} = 0.40$ and $S_{ku} = 0.91$ show that TiN surface is also formed by peaks prevalence ($S_{sk} > 0$) without inordinately high peaks or deep valleys ($S_{ku} < 3$). In this case, positive skewness can have contributed with the adhesion wear by the same interaction mechanism of the tribological pair SiO_2-SGI at 70 m·min^{-1} however under lesser extent.

According to Table 2, center line average roughness (CLA or R_a) for silica coating trended to be greater than for titanium nitride one, but statistically they can be assumed equal given their variability. For this reason, S_p, S_v, S_{sk}, and S_{ku} roughness parameters were chosen to complement the CLA.

4 Conclusions

The tribological behavior of the pin coated by the sol-gel process (SiO_2) was compared to the HSS substrate and the commercial coating (TiN) made by PVD process when sliding against the spheroid graphite iron (SGI), focusing on the mechanical properties, friction, and specific wear coefficients. Tribological evaluation carried out at different sliding speeds in conjunction with wear analysis of tracks and pins allowed to correlate the wear mechanisms occurred. Hereupon, the following conclusions can be drawn:

- Sol-gel process allows producing SiO_2 coatings at low temperatures (400 ºC) with nanometric thickness (~ 500 nm) near one-sixth of those from commercial TiN coatings (~ 3.7 µm). The X-ray diffractograms confirm the amorphous state the SiO_2 film and the formation of a fine crystalline structure of δ-TiN phase for the TiN-coated pin. Basing on the mechanical properties of coatings, the hardness and elasticity modulus of the SiO_2 coating are smaller than that measured for the TiN coating.
- SiO_2 coating presented lower friction and specific wear coefficients (mild wear) at sliding speed of 40 and 55 m·min^{-1} when compared with HSS substrate. However, an increase of the friction and specific wear coefficients at 70 m·min^{-1} sliding speed occurred (severe wear). The TiN coating indicating mild wear behavior for all sliding conditions.
- Wider and deeper wear tracks were found when tribological pair uncoated HSS substrate and SGI were tested (pin-on-disk) regardless of sliding speed while wear tracks produced by SiO_2 and TiN coatings were much smaller and closer mainly at 40 and 55 m·min^{-1} sliding speeds. In particular, SiO_2 coating at of 40 m·min^{-1} showed slightly smaller depths when compared to that generated with TiN coating.
- Adhesion is the predominant wear mechanism on the pins' surface used in the tribological tests. An intense interaction between the HSS substrate pin and the SGI surface resulted in adhesion mechanism for all sliding conditions. Similar result was identified for SiO_2 coating at 70 m·min^{-1} sliding speed. However, the surface interactions between the coated pins and SGI counter-face disk were influenced by different wear behaviors. At sliding speeds 40, 55, and 70 m·min^{-1}, the abrasive wear led to SiO_2 film delamination whilst adhesion mechanism contributed to prevent TiN coating delamination for all sliding speeds.
- Finally, SiO_2 coating demonstrated wear resistance at moderate sliding speeds equivalent to commercial TiN film being a promisor alternative for tribological applications such as HSS cutting tools which work at similar cutting speeds (taps and drills). The sol-gel method is highlighted as a promising technique to improve the tribological behavior when sliding against SGI material. However, SiO_2 coating exhibited some limitations for sliding speeds higher than 55 m·min^{-1}.

Supplementary Information The online version contains supplementary material available at https://doi.org/10.1007/s00170-023-11072-2.

Acknowledgements The authors would like to thank the Postgraduate Program in Production and Mechanical Engineering of the Federal University of Minas Gerais (UFMG), Brazil, for the provision of laboratory facilities. Authors also thank the Tribology Lab of the Metallurgical and Materials Engineering Department at the UFMG. Acknowledge the Center of Microscopy (http://www.microscopia.ufmg.br/) at the UFMG and Polytechnic Institute of Pontifical Catholic University of Minas Gerais (IPUC) for providing technical support and infrastructure for SEM analysis.

Author contribution Natália Pereira was responsible for the conceptualization, experimental work and writing of the manuscript. Bárbara Reis and Anderson Santos were contributed to experimental work and analysis of the data. Manuel Houmard was responsible production of the sol–gel solution, deposition in pins and availability of resources. Marcelo Câmara contributed by conducting the pin-on-disk tests. Manuel Houmard, Marcelo Câmara, Alessandro Rodrigues, and Juan Rubio were responsible for the revision of the manuscript and contributed to the technical discussion of the results. Juan Rubio

was responsible for the supervision of the work and the availability of resources.

Funding The study was financed in by the Coordination for the Improvement of Higher Education Personnel (Coordenação de Aperfeiçoamento de Pessoal de Nível Superior-Brasil (CAPES)-Finance Code 001, and also received financial support from the agencies. The Minas Gerais Research Funding Foundation (Fundação de Amparo à Pesquisa do Estado de Minas Gerais), FAPEMIG, Brazil and National Council for Scientific and Technological (Conselho Nacional de Desenvolvimento Científico e Tecnológico), CNPq, Brazil.

Data availability The authors confirm that the data supporting the findings of this study are available within the article.

Code availability Not applicable.

Declarations

Ethics approval and consent to participate All authors have previously approved this paper and judged that there is no ethical infringement.

Consent to participate and publication All authors would like to declare that they have approved their participation and consent about the publication in this journal.

Competing interests The authors declare no competing interests.

References

1. Dehghanghadikolaei A, Ansary J, Ghoreishi R (2018) Sol-gel process applications: a mini-review. Proc Nat Res Soc 2(02008):1–11. https://doi.org/10.11605/j.pnrs.201802008
2. Amiri S, Rahimi A (2016) Hybrid nanocomposite coating by sol-gel method: a review. Iran Polym J 25(6):559–577. https://doi.org/10.1007/s13726-016-0440-x
3. Wright JD, Sommerdijk NAJM (2001) Sol-gel materials chemistry and applications, 1st edn. CRC Press, New York
4. Tlili B, Barkaoui A, Walock M (2016) Tribology and wear resistance of the stainless steel. The sol-gel coating impact on the friction and damage. Tribol Int 102:348–354. https://doi.org/10.1016/j.triboint.2016.06.004
5. Yazici M, Çomakli O, Yetim T, Yetim AF, Çelik A (2016) Effect of sol aging time on the wear properties of TiO2-SiO2 composite films prepared by a sol-gel method. Tribol Int 104:175–182. https://doi.org/10.1016/j.triboint.2016.08.041
6. Zhang WG, Liu WM, Li B, Mai GX (2002) Characterization and tribological investigation of sol–gel TiO2 and doped TiO2 thin films. Am Ceram Soc 85:1770–1776. https://doi.org/10.1111/j.1151-2916.2002.tb00351.x
7. Yahyaei H, Mohseni M (2013) Use of nano indentation and nanoscratch experiments to reveal the mechanical behavior of sol–gel prepared nanocomposite films on polycarbonate. Tribol Int 57:147–155. https://doi.org/10.1016/j.triboint.2012.08.004
8. Balasubramanian M (2013) Composite materials and processing. 1st edn. CRC Press. https://doi.org/10.1201/b15551
9. Wang D, Bierwagen GP (2009) Sol-gel coatings on metals for corrosion protection. Prog Org Coat 64:327–338. https://doi.org/10.1016/j.porgcoat.2008.08.010
10. Li Y, Xu L, Li X, Shen X, Wang A (2010) Effect of aging time of ZnO sol on the structural and optical properties of ZnO thin films prepared by sol–gel method. Appl Surf Sci 256:4543–4547. https://doi.org/10.1016/j.apsusc.2010.02.044
11. Gunduz B, Cavas M, Yakuphanoglu F (2011) Quality controlling of SiO_2 thin films by sol gel method. The 6th International Advanced Technologies Symposium,6, pp. 569–573. (http://web.firat.edu.tr/iats/cd/subjects/Metallurgy&Material/MSM-118.pdf)
12. Iler RK (1979) The chemistry of silica: solubility, polymerization, colloid and surface properties, and biochemistry, 2nd edn. Wiley, New York
13. Zhang W, Liu W, Wang C (2001) Characterization and tribological investigation of SiO2 and La2O3 sol-gel films. Appl Surf Sci 185:34–43. https://doi.org/10.1016/S0169-4332(01)00568-2
14. Mora LV, Taylor A, Paul S, Dawson R, Taleb WC, W, et al (2018) Impact of silica nanoparticles on the morphogy and mechanical properties of sol-gel derived coating. Surf Coat Technol 342:48–56. https://doi.org/10.1016/j.surfcoat.2018.02.080
15. Liu J, Shi F, Yang D (2004) Characterization of sol-gel-derived TiO_2 and TiO_2-SiO_2 films for biomedical applications. J Mater Sci Technol 20(5):550–554. https://jmst.org/EN/Y2004/V20/I05/550
16. Yang TC, Chin TS, Chang JK, Lin CS (2020) Oxidation resistance of Al2O3/SiO2 nanocomposite coating on hot-dip galvanized steel deposited by chemical immersion and sol-gel coating. Surf Coat Technol 404:126457
17. Zhang L, Wan W, Jiang X, Wang B, Yin L, Agathopoulos S, Xie J, Zhang L, Lu H, Deng L (2022) Enhancement of oxidation and corrosion resistance of flaky carbonyl-iron powder via SiO_2/KH560/PDMS coating applied with sol-gel. Surf Coat Technol 437:128346. https://doi.org/10.1016/j.surfcoat.2022.128346
18. Tschätsch H (2009) Applied machining technology, 8th edn. Springer Dordrecht Heidelberg London New York. https://doi.org/10.1007/978-3-642-01007-1
19. Khlifi K, Larbi ABC (2014) Mechanical properties and adhesion of TiN monolayer and TiN/TiAlN nanolayer coatings. J Adhes Sci Technol 28(85):96. https://doi.org/10.1080/01694243.2013.827094
20. Davis JR (1989) Metals Handbook: Machining. 9 ed. Ohio: ASM
21. Mrkvica I, Neslušan M, Čep R, Sléha V (2016) Properties and comparison of PVD coatings. Tehnički vjesnik 23(2):569–574. https://doi.org/10.17559/TV-20140509105317
22. Fenech J, Dalbin M, Barnabe A, Bonino JP, Ansart F (2011) Sol-gel processing and characterization of (RE-Y)-zirconia powders for thermal barrier coatings. Powder Technol 208:480–487. https://doi.org/10.1016/j.powtec.2010.08.046
23. Rubio JCC, Rezende BA, Vieira LMG, Houmard M (2017) Drilling of aluminium/PE sandwich material with a novel TiO_2-coated HSS drill deposited by sol–gel process. Int J Adv Manuf Technol 92:1567–1577. https://doi.org/10.1007/s00170-017-0138-z
24. Rezende BA, Santos AJD, Câmara MA, Carmo DJD, Houmard M, Rodrigues AR et al (2019) Characterization of ceramics coatings processed by sol-gel for cutting tools. Coatings 9(775):1–12. https://doi.org/10.3390/coatings9110755
25. Pereira NFS, Rubio JCC, Santos AJD, Manuel H, Câmara MA, Rodrigues AR (2019) Drilling of nodular cast iron with a novel SiO_2 coating deposited by sol-gel process in HSS drill. Int J Adv Manuf Technol 105(2019):4837–4849. https://doi.org/10.1007/s00170-019-04429-z
26. ASTM A536-84 (2019) Standard specification for ductile iron castings. ASTM International
27. ASTM G99-05 (2010) Standard test method for wear testing with a pin-on-disk apparatus. ASTM International
28. Batista JCA, Spain E, Housden J, Matthews A, Fuentes GG (2005) Plasma nitriding of Ti6Al4V alloy and AISI M2 steel substrates using D.C. glow discharges under a triode configuration. Surf Coat Technol 200(5–6):1954–1961. https://doi.org/10.1016/j.surfcoat.2005.08.037

29. Oliver WC, Pharr PM (1992) An improved technique for determining hardness and elastic modulus using load and displacement sensing indentation experiments. J Mater Res 7:1564–1583. https://doi.org/10.1557/JMR.1992.1564
30. Pharr GM, Oliver WC (1992) Measurement of thin film mechanical properties using nanoindentation. MRS Bull 17(7):28–33. https://doi.org/10.1557/S0883769400041634
31. Houmard M, Riassetto D, Roussel F, Bourgeois A, Berthomé G, Joud JC et al (2007) Morphology and natural wettability properties of sol-gel derived TiO2-SiO2 composite thin films. Appl Surf Sci 254:1405–1414. https://doi.org/10.1016/j.apsusc.2007.06.072
32. Holmberg K, Matthews A (2009) Coating Tribology, 2nd edn. Elsevier, London
33. Archard JF, Hirst W (1956) The wear of metals under unlubricated conditions. Proc R Soc Lond 236:397–410. https://doi.org/10.1098/rspa.1956.0144
34. Feng X, Zhang Y, Hu H, Zheng Y, Zhang K, Zhou H (2017) Comparison of mechanical behavior of TiN, TiNC, CrN/TiNC, TiN/TiNC films on 9Cr18 steel by PVD. Appl Surf Sci 422:266–272. https://doi.org/10.1016/j.apsusc.2017.05.042
35. Souza PS, Santos AJD, Cotrim MAP, Abrão AM, Câmara MA (2020) Analysis of the surface energy interactions in the tribological behavior of AlCrN and TiAlN coatings. Tribol Int 146:106206. https://doi.org/10.1016/j.triboint.2020.106206
36. Hutchings I, Shipway P (2017) Tribology: friction and wear of engineering materials. 2 ed. Elsevier Ltd: United States
37. Serna MM, Rossi JL (2009) MC complex carbide in AISI M2 high-speed steel. Mater Lett 63:691–693. https://doi.org/10.1016/j.matlet.2008.11.035
38. Carneiro LRS, Garcia DCS, Costa MCF, Houmard M, Figueiredo RB (2018) Evaluation of the pozzolanicity of nanostructured sol-gel silica and silica fume by electrical conductivity measurement. Constr Build Mater 160(1):252–257. https://doi.org/10.1016/j.conbuildmat.2017.11.042
39. Tian B, Yue W, Wang C, Liu J (2015) Surface properties of W-implanted TiN coatings post-treatedby low temperature ion sulfurization. Appl Surf Sci 353(30):1156–1163. https://doi.org/10.1016/j.apsusc.2015.07.017
40. Latella B, Ignat M, Barbé CJ, Cassidy DJ, Bartlett JR (2003) Adhesion behaviour of organically-modified silicate coatings on stainless steel. J Sol-Gel Sci Technol 26(1):765–770. https://doi.org/10.1023/A:1020766725956
41. Xu Z-H, Rowcliffe D (2004) Finite element analysis of substrate effects on indentation behaviour of thin films. Thin Solid Films 447–448(30):399–405. https://doi.org/10.1016/S0040-6090(03)01071-X
42. Bhowmick S, Jayaram V, Biswas SK (2005) Deconvolution of fracture properties of TiN films on steels from nanoindentation load–displacement curves. Acta Mater 53(8):2459–2467. https://doi.org/10.1016/j.actamat.2005.02.008
43. Wouters MEL, Wolfs DP, Van der Linde MC, Hovens JHP, Tinnemans AHA (2004) Transparent UV curable antistatic hybrid coatings on polycarbonate prepared by the sol–gel method. Prog Org Coat 51(4):312–320. https://doi.org/10.1016/j.porgcoat.2004.07.020
44. Jesus MAML, Gomes GHM, Ferlauto AS, Seara LM, Ferreira AM, Mohallem NDS (2019) A systematic study of multifunctional xTiO2/(100–x)SiO2 thin films prepared by sol–gel process. J Sol-Gel Sci Technol 89(2):380–391. https://doi.org/10.1007/s10971-018-4867-8
45. Lai C-M, Lin K-M, Rosmaidah S (2012) Effect of annealing temperature on the quality of Al-doped ZnO thin films prepared by sol–gel process. J Sol-Gel Sci Technol 61(1):249–257. https://doi.org/10.1007/s10971-011-2621-6
46. Twardowska A, Kopia A, Malczewski P (2020) The microstructure, mechanical and friction-wear properties of (TiBx/TiSiyCz)x3 multilayer deposited by PLD on steel. Coatings 10(7):621–638. https://doi.org/10.3390/coatings10070621
47. Bail NL, Benayoun S, Toury B (2015) Mechanical properties of sol–gel coatings on polycarbonate:a review. J Sol-Gel Sci Technol 75(3):710–719. https://doi.org/10.1007/s10971-015-3781-6
48. Grzesik W, Zalisz Z, Krol S, Nieslony P (2006) Investigations on friction and wear mechanisms of the PVD-TiAlN coated carbide dry sliding against steels and cast iron. Wear 261:1191–1200. https://doi.org/10.1016/j.wear.2006.03.004
49. Blau PJ (2009) Friction science and technology: from concepts to applications, 2nd edn. CRC Press, New York
50. Grzesik W, Rech J (2019) Influence of machining conditions on friction in metal cutting process-A review. Mechanik NR 92(4):242–248. https://doi.org/10.17814/mechanik.2019.4.33
51. Rabinowicz E (1995) Friction and wear of materials, 2nd edn. Wiley, Canada
52. General catalogue: turning, milling, tapping and drilling. Tübingen, Germany: Walter Tools; 2017
53. López AJ, Ureña A, Rams J (2011) Wear resistant coatings: silica sol-gel reinforced with carbon nanotubes. Thin Solid Films 519:7904–7910. https://doi.org/10.1016/j.tsf.2011.05.076
54. Fillot N, Iordanoff I, Berthier Y (2007) Wear modeling and the third body concept. Wear 262:949–957. https://doi.org/10.1016/j.wear.2006.10.011
55. Österle W, Dörfel I, Prietzel C, Rooch H, Cristol-Bulthé AL, Degallaix G, Desplanques Y (2009) A comprehensive microscopic study of third body formation at the interface between a brake pad and brake disc during the final stage of a pin-on-disc test. Wear 267(5–8):781–788. https://doi.org/10.1016/j.wear.2006.03.004
56. Czichos H, Habig K-H (2010) Tribologie Handbuch, vol 3. Vieweg+Teubner Verlag, Wiesbaden
57. Abedi HR, Fareghi A, Saghfian H, Kheirandish SH (2010) Sliding wear behavior of a ferritic–pearlitic ductile cast iron with different nodule count. Wear 268:622–628. https://doi.org/10.1016/j.wear.2009.10.010
58. Hassan AD, Alrashdan A, Hayajneh MT, Mayyas AT (2009) Wear behavior of Al–Mg–Cu–based composites containing SiC particles. Tribol Int 42:1230–1238. https://doi.org/10.1016/j.triboint.2009.04.030
59. Sedlacek M, Gregorcic P, Podgornik B (2016) Use of the roughness parameters S_{Sk} and S_{ku} to control friction-a method for designing surface texturing. Tribol Transact 60(2). https://doi.org/10.1080/10402004.2016.1159358
60. Komvopoulos K (1996) Surface engineering and microtribology for microelectromechanical systems. 200(1–2):305–327. https://doi.org/10.1016/s0043-1648(96)07328-0
61. Krolczyk GM, Maruda RW, Krolczyk JB, Nieslony P, Wojciechowski S, Legutko S (2018) Parametric and nonparametric description of the surface topography in the dry and MQCL cutting conditions. Measurement 121:225–239. https://doi.org/10.1016/j.measurement.2018.02.052
62. Miyoshi K (1990) Fundamental considerations in adhesion, friction and wear for ceramic-metal contacts. Wear 141:35–44. https://doi.org/10.1016/0043-1648(90)90190-L